Research Article

iMedPub Journals
www.imedpub.com

Nano Research & Applications
ISSN 2471-9838

2021
Vol.7 No.9:43

Selective Cytotoxicity of Camellia Sinensis Green Synthesized Magnetic Nanoparticles against the MCF 7 Tumor Cell Line and their Molecular Activity

Bandana B[1], Debasish P[2]* and Adyasa S[1]

1 University Department of Pharmaceutical Sciences, Utkal University, Bhubaneswar, India
2 Department of Pharmacy Science, Creighton University, Medical Centre, Omaha, NE, USA

***Corresponding author:**
Dr. Debasish Pradhan

Department of Pharmacy Science, Creighton University, Medical Centre, Omaha, NE, USA.

E-Mail: deba_udps@yahoo.co.in

Citation: Bandana B, Debasish P, Adyasa S (2021) Selective Cytotoxicity of Camellia Sinensis Green Synthesized Magnetic Nanoparticles against the MCF 7 Tumor Cell Line and their Molecular Activity. Nano Res Appl Vol.7 No.9:43

Abstract

Iron Oxide Nanoparticles (IONPs) have received recognition to be used in cancer treatment. In this investigation analysis, IONPs have been biosynthesized the usage of naringenin (NAR). We examined the anti-breast cancer role of biogenic IONPs via transcriptome analysis with the use of RNA sequencing, and IONPs mechanisms to regulate the development of breast cancer cells. Synthesized IONPs have been characterised via use of UV-Vis, XRD, FTIR, DLS, and TEM. The IONPs were in sizes of 2-10 nm and spherical in shape. Cytotoxicity studies indicate that at low concentrations, the IONPs in MCF 7 breast cancer cells are very much efficient. The proliferation and viability of breast cancer cells analyzed with 5 μg/mL biogenic IONPs were decreased by 50%. Reduced dead-cell protease activity, enhanced leakage of lactate dehydrogenase, malondialdehyde, reactive oxygen species generation, and ATP generation is observed. This DNA damage and impaired mitochondrial function progress to cell death. The IONPs up-regulate and down-regulate the most top-ranked biological processes of cell-cycle regulation and oxidation-reduction. The KEGG research has shown that IONPs up-regulated GADD45G in the p53 pathway. Therefore, the tumor-suppressive effects of IONPs were mediated by cell death followed by mitochondrial aberrancy, cell-cycle arrest, and DNA damage following abnormal regulation of p53 effector proteins. It is interesting to note that, this research is the first study that demonstrates molecular pathways analysis and cellular responses of IONPs in MCF 7 breast cancer cells.

Keywords: Iron oxide nanoparticles; Cell viability; Oxidative stress; DNA damage; Kegg analysis; Biological pathways

Received: August 25, 2020; **Accepted:** September 18, 2021; **Published:** September 25, 2021

Introduction

According to the International Agency for Research on Cancer, breast cancer is the second most frequently occurring cancer in females and widely diagnosed malignancy in males [1]. With approximately 1.45 million new cases reported in 2012, breast cancer is the third most frequent malignancy and the fourth major cause of cancer related deaths globally. It has been estimated that 2.4 million breast cancer cases will rise to 1.35 million for men and 1.07 million for women by 2035 [2]. Therefore, it is desirable to minimize the breast cancer [1,3]. For researchers, gastroenterologists, and oncologists, treating breast cancer remains a major challenge. 5-fluorouracil is the only drug accepted for the treatment of advanced breast cancer. [4]. Even though chemotherapy is still a conventional treatment, it has some adverse effects, including nausea, loss of appetite, vomiting, constipation, and alopecia. As a result, new therapeutic approaches are required [5].

Iron Oxide Nanoparticles (IONPs) have recently been used as strong broad spectrum antibacterial agents in textiles, food storage containers, antiseptic sprays, bandages, and anti-cancer medicines due to their unique qualities. [6,7]. IONPs are effective anticancer agents. Low concentrations of IONPs cause DNA

© Under License of Creative Commons Attribution 3.0 License

damage and chromosomal disorder without substantial toxicity [8,9]. Lima et al. found no evidence of genotoxicity in human culture cells treated with 10 mg/mL of capped IONPs with an average size of 6-80 nm. IONPs are known to associate with cells and to manage different cellular responses in both active and passive ways [10]. By suppressing the phosphorylation of protein kinase B/Akt, Gurunathan et al. revealed the antiangiogenic properties of IONPs in vascular endothelial cells, which depicts equal efficacy to a natural antiangiogenic molecule called as pigment epithelium-derived factor [11].

SriRam et al. revealed exceptional cytotoxicity capacity against Dalton's Lymphoma Ascites (DLA) and DLA-induced tumours in mice, with considerably better survival rates in the tumour mouse model as compared to the untreated group [12]. After penetrating the cells through the endocytic route endosomes of low concentrations of poly (N-vinyl-2-pyrrolidone)-coated IONPs reduces the viability of acute myeloid leukemia cells and K562 cells in a dose-dependent manner [13]. Importantly, IONPs have anti-cancer and cytotoxic effects on cancer cells via various mechanisms, such as inducing cellular apoptosis via mitochondrial dependent and mitochondrial independent pathways against various types of cancer cells, such as human breast cancer cell lines (MCF-7, MDA-MB-231), liver (HepG2), lung (A549), and skin and oral cancer cell lines (HT144), via the leakage of lactate dehydrogenase, impairment of mitochondrial dysfunction, and the Reactive Oxygen Species (ROS) generation [14-19].

However, the anticancer activity of IONPs is affected by a variety of factors, including their shape, size, and surface coatings, as well as surface charge, cell types, and reducing agent utilised to synthesize the IONPs. While conventional, physical, and chemical procedures are straightforward, the processes consume energy and need the use of harmful compounds [15]. Synthetic capping agents, like polyethylene glycol, polyvinyl pyrrolidone, and polyvinyl alcohol, are also toxic and poisonous. As a result, interest in utilising biomolecules as capping agents for IONPs has elevated [20].

With the emergence of next generation sequencing technologies, such as RNA sequencing (RNA-Seqe), which potentially substitute complementary DNA (cDNA) microarrays as the preferred approach for gene expression profiling of cells and tissues, the transcriptomics field has advanced fast in recent years [21,22]. Transcriptome analysis, in conjunction with bioinformatics data-mining techniques, could be utilised concurrently for studying several genes/targets and determine action mechanism following treatments. RNA-Seqe is a helpful technique for detecting differentially expressed genes after treatment with several drugs [23]. When compared to whole-genome sequencing, RNA-Seqe has several advantages: it focuses on transcribed regions of genomes, it is free of probe-specific hybridization of microarrays, and it has broad coverage, allowing for unbiased identification of both coding and noncoding novel transcripts, as well as low-abundance transcripts [23-25]. To overcome the restrictions of conventional approaches, we developed IONPs with well controlled morphological and physicochemical properties for physiological application in humans, thus, used biological method to synthesise IONPs utilising a pure aqueous solution of NAR.

Few studies have investigated into the synthesis of IONPs using pure flavonoid reduction of Iron Oxide. In this study, we used MCF 7 cell lines to systematically examine the anticancer potential of NAR stabilised IONPs, as well as the mechanism of IONPs in regulating the development of breast cancer cells using the RNA-Seqe technique. Although IONPs have been proven to reduce cell viability and proliferation in various cancer cells, the method by which they do so remains unknown. As a result, gene expression profiling could be employed as a new method for detecting molecular pathways in interactions with nanoparticles and biological systems. Furthermore, our methodology can predict IONP toxicity mechanisms in cancer cells.

Materials and Methods

Material

MCF 7 breast cell lines were purchased from National Centre for Cell Science (NCCS), Pune, India. Life Technologies/Gibco (Grand Island, NY, USA) supplied trypsin-EDTA, penicillin-streptomycin, Dulbecco's Modified Eagle's Medium (DMEM), and 1% antibiotic-antimycotic. Sigma-Aldrich (St. Louis, MO, USA) provided *in vitro* toxicity assay kit and foetal bovine serum. Unless otherwise specified, all chemicals including iron oxide nitrate were bought from Sigma-Aldrich.

Synthesis and characterization of IONPSs

The synthesis and characterization of IONPs were carried out as described previously [17]. The IONPs were synthesized using NAR, dissolved in DMSO. IONPs were synthesized by incubating 50 M NAR in 100 mL of water containing 2 mM $Fe(NO_3)_3$, for 1 hr at 37°C. The development of IONPs in the reaction mixture was attributed to the colour change from pale yellow to dark yellowish brown.

Cell viability and cell proliferation

A Cell Counting Kit-8 was used to determine cell viability (CCK-8, CK04-01, Dojindo Laboratories, Kumamoto and Japan). Cell proliferation was measured in accordance with the manufacturer's instructions (Roche, Basel, Switzerland). MCF 7 cells was placed on 96-well plates with varying concentrations of IONPs. After 24 hrs of culture at 37°C and 5% CO_2 in a humidified incubator, CCK-8 solution (10 μL) were added into each well, and the plate was incubated for next 2 hr at 37°C. At 450 nm, absorbance is recorded with a microplate reader (Multiskan FC, Thermo Fisher Scientific, Inc, Waltham, MA, USA)

Membrane integrity

Using an LDH Cytotoxicity Detection kit, the membrane integrity of MCF 7 cell lines was evaluated. Cells were exposed for 24 hrs to varying concentrations of IONPs. Following that, 100 μL of cell free supernatant from each well was transferred in triplicate to the wells of a 96-well plate, followed by 100 μL of LDH reaction mixture. After 3 hr, 100 μL of cell free supernatant was transferred in triplicate from each well to the well of 490 nm microplate reader.

Assessment of dead-cell protease activity

As previously stated, dead-cell protease activity was measured. In MCF 7 cells, the cytotoxicity test was used to determine the cytotoxicity of IONPs. An intracellular protease reaction using a luminogenic peptide substrate was used to assess cytotoxicity (alanyl-alanylphenylalanyl-aminoluciferin). Luminescence is evaluated with a Luminescence Counter (Perkin Elmer, Waltham, MA, USA).

Determination of intracellular ROS

MCF 7 cells were exposed to IONPs for 24hr. ROS was measured using previously model based on the intracellular peroxide dependent oxidation of 20, 70-Dichlorodihydrofluoresceindiacetate (DCFH-DA, Molecular Probes, Eugene, OR, USA) to generate the fluorescent molecule 20, 70-Dichlorofluorescein (DCF).

Measurement of MDA

Oxidative stress indicators like Malondialdehyde (MDA) was assessed in accordance with the manufacturer instructions. The cells were cultivated in 75cm^2 culture flasks and exposed to different concentrations of IONPs for 24 hrs. The cells were extracted in chilled Phosphate-Buffered Saline (PBS) by scraping and washing twice with saline, followed by centrifugation at 4˚C for 6 minutes at 1500 rpm. To obtain the cell lysate, the cell pellet was sonicated at 15 W for 10 sec (thrice). The generated supernatant was kept at -70˚C until evaluation.

Jc-1 assay

MCF 7 cells undergoes treatment with IONPs for 24 hrs. JC-1, a cationic fluorescent dye, is used for measuring the changes in Mitochondrial Membrane Potential (MMP) (Molecular Probes). The fluorescence of JC-1 accumulates and JC-1 monomers was measured using a Gemini EM fluorescent microplate reader at excitation wavelengths of 488 nm and emission wavelengths of 583 and 525 nm (Molecular Devices, Sunnyvale, CA, USA).

Measurement of ATP

ATP levels in MCF 7 cells subjected to various concentrations of IONPs for 24 hrs were measured according to the manufacturer instructions (Sigma-Aldrich, Catalog Number MAK135).

Tunel analysis

The terminal deoxynucleotidyltransferase-mediated dUTP nick end labelling (TUNEL) method was used with an insitu detection kit (Promega, Madison, WI, USA) to detect apoptotic cells in groups undergoes treatment with IONPs (5 μg/mL). MCF 7 cells were plated in 6 well plates and incubated with IONPs (5 μg/mL) for 24 hrs and TUNEL analysis is performed to determine cell apoptosis. Nikon Eclipse E400 fluorescent microscope (Nikon 40 Plan 40/0.65, Tokyo, Japan) was used to examine the samples. The difference in the no. of TUNEL-positive cells between the control and experimental samples was statistically analysed.

RNA-seqe and downstream bioinformatics analysis

Total RNA was extracted using the TRIzol reagent according to the manufacturer instructions (Thermo Fisher Scientific, Waltham, MA, USA). Total RNA quality was determined utilizing the Agilent 2100 bioanalyzer (Agilent Technologies, Santa Clara, CA, USA) and the RNA 6000 Nano LabChip kit. RNA-Seqe libraries was created with the Illumina® TruSeq stranded total RNA Library Prep Kit v2 (San Diego, CA, USA) and sequenced with an Illumina® Hiseq2500 to yield 150-base paired end reads. Each sample had a sequencing depth of more than 20 million reads. The readings were aligned using TopHat 2.0.13 default settings to GRCh37, and then assembled using Ensembl v75 annotations by Cufflink 2.2.1. The abundance of transcripts were measured in fragments per kb of exon per million fragments mapped (FPKM). Differentially expressed genes were found when the FPKM >2 and fold change >2. The RNA-Seqeuence data can be found on the GEO website (GSE100687). The DAVID (v6.8) approach was used to enrich biological processes and KEGG pathways. Scatter plots and Gene Ontology terms were created using the R package (v3.3.2) and the GO plot programme (version 1.0.2, respectively). To predict the expression patterns of representative genes, the integrative genomics viewer was employed.

Statistical methods

At the least 3-independent experiments were carried out, and the data is expressed as the mean ± standard deviation for all duplicates within an individual experiment. Data were analysed using the Graph-Pad Prism analysis programme (GraphPad, Inc, La Jolla, CA, USA) to discover differences between groups, denoted by an asterisk, using a t-test, multivariate analysis, or one-way analysis of variance, and for multiple comparisons the Tukey test.

Results and Discussion

Synthesis and characterization of IONPs using NAR:

Pure aqueous solution of NAR (50 M) were combined with 2 mM Iron Oxide nitrate and incubated at 37˚C for 1 hour to synthesize IONPs. NAR is a flavonoid with effective antibiotic, anticancer, and antiinflammatory properties that act against different types of carcinogenic cells [26-28]. Colour generation occurs quickly in this mixture, most likely due to the interaction between iron oxide ions and NAR [12,28]. UV-visible spectroscopy (UV-vis) was used to confirm the synthesis of IONPs. At 442 nm a single absorption peak was detected in the UV-visible spectrum, indicating that the synthesized IONPs were pure **(Figure 1A).** IONPs exhibit strong surface plasmon resonance in aqueous solution and their absorbance spectra is affected by their size, shape, and morphology. Pure flavonoids are used in the synthesis of IONPs, which is quicker than using the whole plant extract and it prevents the incorporation of contamination [28-30].

X-ray Diffraction (XRD) analysis was used to analyze the crystalline structure & surface morphology of the synthesized IONPs and it was analyzed between the range of 20˚ to 80˚. The XRD pattern of IONPs produced by reacting aqueous Iron Oxide salt with NAR is depicted in **Figure 1B.** The XRD pattern revealed typical IONP peaks, indicating that the IONPs are crystalline in nature. High-intensity peaks of IONPs synthesised utilising NAR was detected

© Under License of Creative Commons Attribution 3.0 License

at approx 39°, 45°, and 77°, corresponding to (111), (200), and (311) Bragg reflections, respectively, and are the precise peak positions for Iron Oxide's face centered cubic lattice structure. For IONPs synthesised using NAR, the average particle size obtained from the XRD pattern using the Scherrer equation is around 7 nm. Our findings are consistent with previous reports of IONPs production employing plant extracts [14], different flavonoids such as hesperidin, naringenin, and diosmin [28], and Ocimum Sanctum leaf extracts and its derivative, quercetin [30].

We performed Fourier-Transform Infrared (FTIR) spectroscopy to analyze whether NAR was responsible for reducing Iron Oxide ions to IONPs. The synthesized IONPs displayed peaks at approx 1641, 2111, and 3269 cm^{-1}, which corresponds to the groups C=C, C≡C, and amine N-H/O-H stretching vibrations, respectively, as shown in **Figure 1C.** This denotes that NAR was responsible for reducing Iron Oxide ions to IONPs, which strongly corresponds to the same functional groups found in quercetin is important for reducing Iron Oxide into IONPs [30, 31]. Also, IR spectra shows a significant stretching of the O-H bond as a strong signal peak between 3000 and 3500 cm−1 [14,15,17]. In a previous study, flavonoids was utilised as reducing agents to synthesize IONPs indicated a strong signal for an O-H bond [32].

Although Transmission Electron Microscopy (TEM) can be used to evaluate particle size and morphology, it is essential to determine particle size in solution before analysing toxicity in cells. To analyse a large number of particles in a single solution, the Dynamic Light Scattering (DLS) approach is used [15,17]. **Figure 1D** depicts the particle size distribution measured by DLS for the IONP combination. According to the particle-size histogram, IONPs ranged in size from 1 to 10 nm, with a mean diameter of 7 nm. The DLS intensity analysis indicated a single broad and sharp peak with an average size of 7 ± 1 nm. We utilized TEM, to analyse the consistency of particle sizes and morphologies. **Figure 1E** shows a TEM picture of IONPs in the micrograph with spherical shape and homogeneous particle size distribution, with sizes similar to those analysed using DLS. The results of size measurement of IONPs from TEM images are summarised in **Figure 1F**. Both TEM and DLS investigations revealed that the produced IONPs were 7 nm in size. The sizes of nanoparticles synthesised from hesperidin, diosmin, and NAR was determined by Sahu et al. to be around 5 to 50 nm, 5 to 40 nm, and 20 to 80 nm, respectively [28]. IONPs formed from hesperidin and NAR were oval-shaped and polydispersed, whereas diosmin-derived IONPs were hexagonal-shaped. Using citrus plant extract, Prathna et al. generated IONPs with an average size of 50 nm [33]. Tulsi extract- and quercetin-mediated IONP production, according to Jain and Mehata, had an average size of 14.6 nm and 11.35 nm, respectively [30]. Our outcomes indicate that NAR produces smaller particles, which easily permeate cells and releases Iron Oxide ions more quickly than larger particles.

Effect of IONPs on cell viability and proliferation of MCF 7 Cells

MCF 7 cells were treated with several IONP concentrations and their cell viability was assessed based on mitochondrial activity to determine the toxic effects of IONPs. After 24hrs of exposure, mitochondrial activity was reduced in response to a concentration of 2 μg/mL, and cell viability was quickly reduced when IONP concentrations were elevated from 2 to 10 μg/mL. **(Figure 2A).** At 4 to 10 μg/mL IONPs, mitochondrial activity is significantly reduced to 50% in MCF 7 cells treated to 5 and 4 μg/mL IONPs. Mitochondrial activity in IONP-exposed cells was significantly reduced at this time and dose. Miethling-Graff et al. [34] investigated the size-dependent (10, 20, 40, 60, and 100 nm) effects of IONPs in the human LoVo cell line and discovered that cellular uptake and toxicity were size-dependent, with small particles easily penetrating the cells, whereas larger particles such as 100-nm particles did not. Likewise, in the human breast cancer cell line MCF 7, para-hydroxybenzoatetetrahydrate (SPHT)-assisted IONP production inhibited cell viability in a dose dependent and time dependent manner. After 24hrs of treatment, cells that were exposed to SPHT-IONPs (8 μg/mL) showed a 50% suppression of cell proliferation [35]. When compared to synthetic IONPs and $Fe(NO_3)_3$, plant-assisted IONPs exhibited greater antiproliferative activities against MCF 7 cells at a minimal

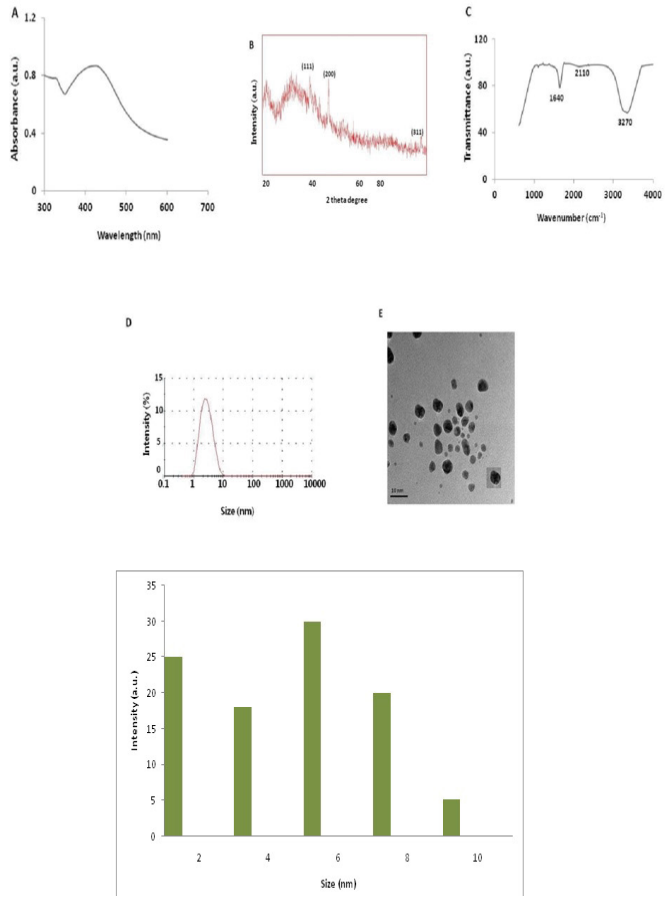

Figure 1 Synthesis and characterization of Iron Oxide Nanoparticles (IONPs). (A) UV–Vis spectra of IONPs, (B) XRD pattern of IONPs, (C) FTIR spectra of IONPs, (D) Size distribution analysis of IONPs using DLS, E) TEM images of IONPs and (F) Particle size distributions from TEM images. The diameter of IONPs was determined from more than 200 particles.

concentration of about 450 nM [36]. The anti-proliferative effects of Abutilon indicum-assisted IONPs on COLO 205 (human colon cancer) and MDCK (normal) cells were dose-dependent [37].

Then, using BrdU incorporation during DNA synthesis, we evaluated at the dose-dependent effects of different IONP concentrations on cell proliferation. MCF 7 cells subjected to various concentrations of IONPs exhibited considerably lower proliferation rates as compared to control cells, which is consistent with the cell viability analysis results **(Figure 2B).** After 24 hrs exposure to various concentrations of IONPs, the proliferation rate was measured in comparison to non-exposed control cells. The results indicate that as the doses increased, the rate of proliferation reduced. Breast cancer cells, lung cancer cells, ovarian cancer cells, neuroblastoma cells all showed anti-proliferative effects in the presence of IONPs. HT-29 appears to be more sensitive than MCF 7 cells among the two cell lines studied. As a result, additional research focused on MCF 7 cells [8,38,17,15,39].

IONPs increase cytotoxicity in MCF 7 Cells

Lactate Dehydrogenase (LDH) leakage assay is a cytotoxicity assay for determining cytotoxicity based on the leakage of intracellular molecules through damaged plasma membranes. LDH is a soluble cytoplasmic enzyme found in almost all cells that is released into the extracellular space when the plasma membrane is damaged [16,40,41]. To identify LDH leakage into culture medium, cells were treated for 24 hrs with various concentrations of IONPs (2-10 μg/mL), and leakage was evaluated as the quantity of formazan product generated by standard spectroscopy. LDH activity was measured at 495 nm using an LDH cytotoxicity kit. As expected, increasing IONP doses resulted in LDH leakage that was directly proportional to IONP dosage and improved cytotoxicity **(Figure 3A),** denoting that cells experiencing accidental cell death due to IONPs, swelling and losing membrane integrity before switching down and releasing their intracellular contents into the surrounding environment. These findings suggest that elevated IONP concentrations disrupt cellular membrane integrity. Our findings support the previous reports that IONPs lead to LDH leakage in many cancer-type cell and Non-Cancerous Cell types, including human breast cancer cells, lung cancer cells, ovarian cancer cells, neuroblastoma cells, microvascular endothelial cells, male somatic cells, spermatogonial stem cells, and neural stem cells [14, 38, 17, 16, 39, 42, 8, 43]. The results indicate collectively that the low viability in IONP-exposed MCF 7 cells coincides with increased LDH leakage and significant cytotoxicity. While a number of assays for measurement of cell viability and toxicity have been developed, proteolistic actions associated to cellular death are truly sensitive and are cytotoxic and dependent on membrane integrity.

Consequently, in MCF 7 cells exposed to various doses of IONPs, we assessed their impact on dead-cell protease activity, their cell viability was measured according to manufacturer instructions (Proméga Corp, G9292, WI, USA), and the method reported previously [44]. With increasing IONP concentrations MCF 7 cells treated with IONPs showed a lower viability **(Figure 3B).** The results reveal a substantially reduction in the viability of MCF 7 cells.

Effect of IONPs on ROS generation and Malondialdehyde (MDA)

In the presence of oxygen species, iron oxide ions play a significant role in catalysing ROS generation, and IONPs can induce oxidative stress in a range of cellular systems by producing ROS, including

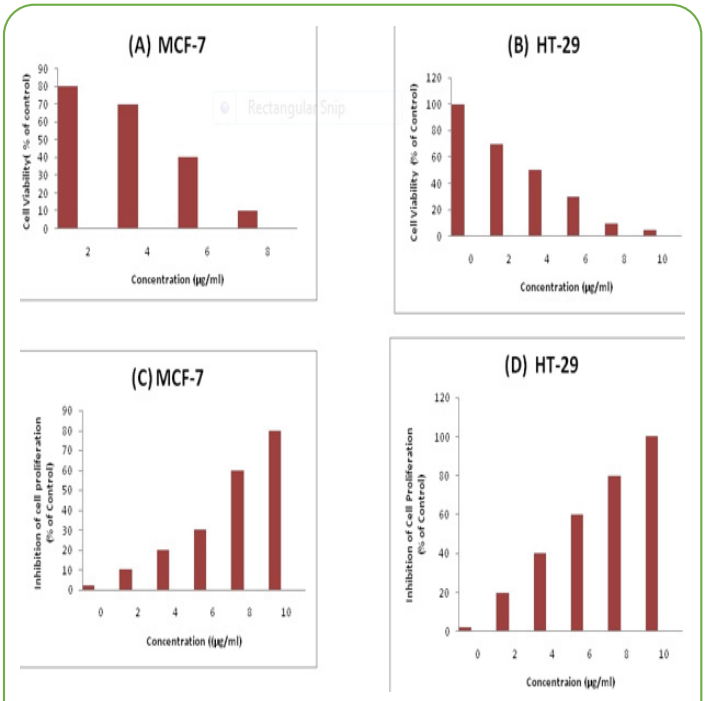

Figure 2 Cell viability and proliferation assessment of IONPs in MCF 7 and HT-29 cells. (A and B) cell viability of MCF 7 and HT-29 cells, (C and D) Cell proliferation of MCF 7 and HT-29 using a BrdU cell proliferation assay. The findings are expressed as the mean ± standard deviation of three separate independent experiments. There was a significant difference is determined by a Student's t-test (* p <0.05).

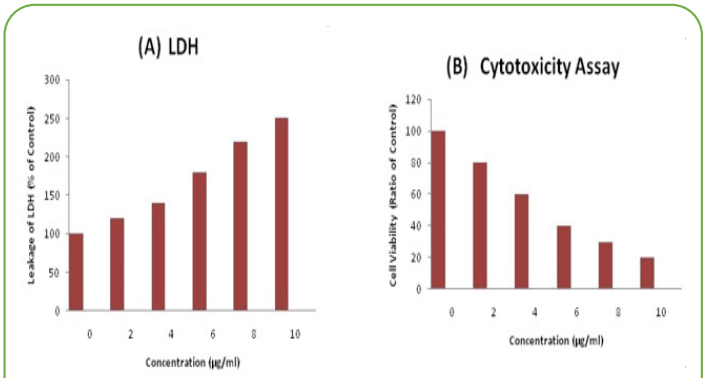

Figure 3 (A) Measurement of LDH leakage activity and (B) measurement of cell-death protease activity using the CytoTox-Glo cytotoxicity assay. The results are expressed as the mean ± standard deviation of three independent experiments. There was a significant difference is determined by a Student's t-test (* p <0.05).

© Under License of Creative Commons Attribution 3.0 License

human ovarian cancer cells [16], lung cancer (A549) cells [45,46], and human neuroblastoma cells [39]. MCF 7 cells were treated with different concentrations of IONPs for 24 hrs to know the influence of IONPs on ROS formation, and ROS generation was evaluated using an H2DCF-DA assay. When compared to the control, increasing IONP concentrations (2-10 μg/mL) significantly increased ROS levels at concentrations over 6 μg/mL after 24 hrs of exposure **(Figure 4A).** The amount of ROS produced in response to IONPs treatment was substantially higher than in control cells. Greater concentrations, up to 2-3-fold higher ROS levels, were the most significant effects at all concentrations examined. Miethling-Graff, et al. [34] found that ROS formation was size-dependent in the human LoVo cell line, with small particles producing excess ROS than bigger ones. COLO205 cells subjected to IONPs produced much more ROS than untreated control cells, according to Mata, et al. [37].

The primary anticancer effect of IONPs is the induction of apoptosis and autophagy via a variety of molecular mechanisms, including a significant decrease in cell viability and motility, impairment of matrix metalloproteinase-2 and -9 activities, and the promotion of ROS production, which induces cell death via apoptosis and autophagy [47]. The potential toxicity of IONPs is determined by the formation of Reactive Oxygen Species (ROS), the depletion of antioxidant defence systems, and the loss of mitochondrial membrane potential [44]. ROS formation in human breast cancer cells is influenced by the surface coating of IONPs by different biological reducing agents, such as bacterial cellular extracts and fungal cellular extracts. For example, IONPs made with fungal extracts generated more ROS than IONPs made with bacterial cellular extracts, implying that coating materials influence ROS formation and, ultimately, cell death [14]. IONPs coated with chitosan-derived polysaccharide, on the other hand, displayed antibacterial action while causing no toxicity in eukaryotic cells [48]. Our investigation imply that IONPs produce significant amounts of ROS, which may induce apoptosis by disrupting the balance between the oxidant and antioxidant enzyme systems, causing cellular redox to change [44].

ROS-mediated oxidative stress is a common cause of cell death, and it is used to control the cellular processes like proliferation, apoptosis, and necrosis based on the amounts of oxidant and antioxidant enzymes present [49]. The disturbance between pro oxidants and antioxidants occurs when cancer cells are exposed to chemotherapeutic drugs, cytotoxic agents, and nanoparticles. As a result, we measured MDA levels in MCF 7 cells that had been exposed to various amounts of IONPs for 24hrs. Lipid peroxidation (LPO) was determined via the reaction of Malondialdehyde (MDA) with thiobarbituric acid to form a colorimetric (533 nm)/ fluorometric (excitation and emission wavelengths of 533 and 554 nm, respectively) product, whose quantity was proportional to that of MDA. The findings showed that IONPs enhanced MDA levels in human prostate cancer cells, and that increasing IONP concentrations dramatically increased MDA levels **(Figure 4B).** Long-term exposure to IONPs in lung cells up-regulated the gene expression of antioxidant enzymes such as glutathione-S-transferase enzymes i.e., involved in clearing lipid peroxidation products, according to Gliga et al [50]. Ferroptosis, which is emerging as a form of controlled cell death, is characterised by lipid peroxidation, which is a source of free radical generation and also characteristic of ferroptosis. Overall, our data indicate that IONPs cause oxidative stress by oxidising lipid biomolecules.

IONPs induce mitochondrial dysfunction and reduce ATP generation in MCF 7 Cells

The loss of mitochondrial function is an important factor and predictor of cell apoptosis that may be evaluated by monitoring changes in Mitochondrial Membrane Potential (MMP). Using cationic fluorescent dyes, we evaluated MMP in IONP-treated MCF 7 cells [47]. MCF 7 cells were treated with different concentrations of IONPs for 24 hrs to determine effect of IONPs on MMP, and then the MMP status was measured. When compared to control cells, the treated cells showed significant **changes (Figure 5A).** These findings show that incubation with IONP for 24 hrs significantly decrease MMP, and the reductions in cell viability and toxicity were linked to MMP loss and enhanced ROS accumulation. Increased ROS production leads to mitochondrial-dependent cell death pathways via the formation of mitochondrial permeability transition holes in previous studies [51,52].

ROS production increases due to mitochondrial membrane depolarization, which is an important element in activating intrinsic cell-death pathways [16, 46]. As a result, MMP deficiency suggests that mitochondrial depolarization is a key mechanism of IONP-induced toxicity, involving one or more signalling cascades with crosstalk between the mitochondrion and other cellular components [45,53,54]. The cytotoxicity of IONPs was elevated due to cellular uptake by MCF 7 cells via an MMP alteration. Flow cytometry examination of IONP-treated MCF 7 cells using JC-1 (Molecular Probes, Eugene, OR, USA) dye validated the change in MMP. In healthy cells, the mitochondrial stain JC-1 can aggregate and emit red fluorescence at high membrane potential, whereas in apoptotic cells, JC-1 remains in the form of green fluorescent monomers due to mitochondrial membrane depolarization. **Figure 5B** shows the change in MMP in MCF 7 IONP-induced cells.

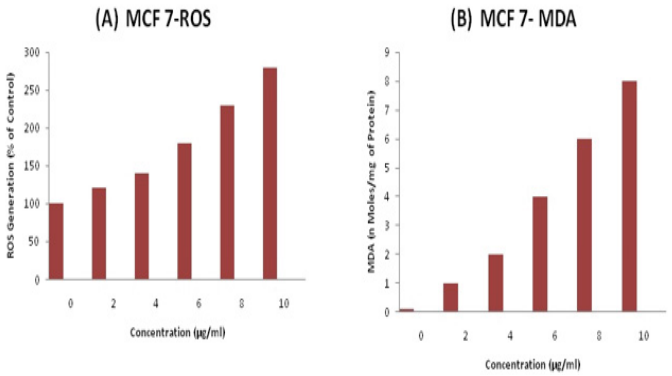

Figure 4 Effect of IONPs on Reactive Oxygen Species (ROS) generation. A) MCF 7- ROS generation measured using (DCFH-DA) and B) MDA levels in MCF 7 cells. The results are expressed as the mean ± standard deviation of three independent experiments. There was a significant difference is determined by a Student's t-test (* p <0.05).

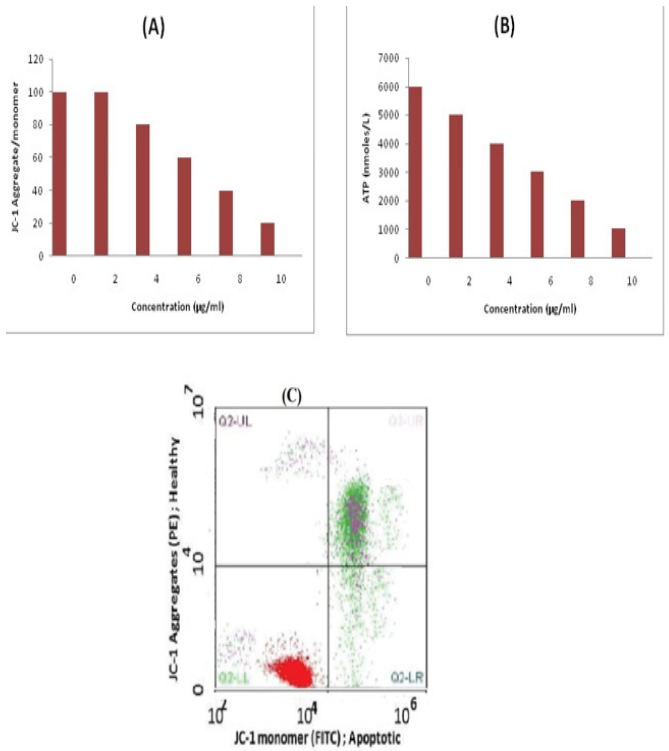

Figure 5 Measurement of Mitochondrial Membrane Potential (MMP) and ATP. (A) Change in MMP using the cationic fluorescent dye, JC-1 (Molecular Probes, Eugene, OR, USA), (B) Flow cytometric analysis of the MMP using the JC-1 dye in MCF 7 cells and (C) Measurement of ATP. The results are expressed as the mean ± standard deviation of three independent experiments. There was a significant difference is determined by a Student's t-test (* $p < 0.05$).

This signifies that apoptosis induction by IONPs is linked to the mitochondrial tract.

We next assessed ATP levels in both IONP-treated and untreated cells to see if the loss of MMP affects ATP synthesis in IONP-treated cells. The ATP level was measured according to the manufacturer's instructions (Sigma-Aldrich, St. Louis, MO, USA, Catalog Number MAK135) in MCF 7 cells exposed to IONPs for 24 h. Damage to mitochondria causes reduced or inefficient energy generation, potentially affecting ATP production or ATP-dependent cellular functions [55]. When compared to controls, IONP-treated cells produced considerably less ATP, as expected **(Figure 5C).** Interestingly, higher IONP concentrations resulted in lower ATP synthesis. The findings revealed that IONP concentration and ATP generation had a direct linear connection. As a result, the cells seems to be vulnerable to mitochondrial toxicants like IONPs that is analogous to drug-induced mitochondrial poisoning and mitochondrial inherited disorders [56].

IONPs induce apoptosis

Oxidative stress and cell death are caused by high ROS levels [57]. Our lab and other research groups previously demonstrated that IONP-induced cytotoxicity is primarily caused by oxidative stress, which induces cell apoptosis by activating the intrinsic apoptosis, autophagy, or both pathways [15,39,46,53]. We used terminal deoxynucleotidyltransferase-mediated dUTP nick end labelling (TUNEL) analysis to see if IONP-induced cell death is caused by apoptosis. Through numerous processes generating macromolecular damage, such as lipid peroxidation, DNA fragmentation, protein denaturation, and mitochondrial malfunction, oxidative stress is a crucial component in the activation of apoptosis in cancer cells [53]. ROS acts as signalling molecules, promoting cell division and generating oxidative DNA damage [51,58].

The best method for evaluating IONP-induced apoptosis tends to be measuring DNA fragmentation. MCF 7 cells was analysed with the half maximum inhibitory concentration (IC50) of IONPs and a DNA-fragmentation test was performed to detect apoptotic characteristics generated by IONPs. **Figure 6** shows the results, which show a remarkable number of positively marked cells, indicating apoptotic DNA fragmentation. Few or no apoptotic cells were found in control cultures. Cell shrinkage, widespread plasma membrane bleb, chromatin condensation, and the dissociation of cell fragments into apoptotic bodies are all characteristics of apoptosis [59]. Cancer cell lines analysed with IONPs displayed the similar "laddering" pattern as suggested by DNA fragmentation in this study [14]. The accumulation of Iron Oxide particles inside the nucleus during DNA fragmentation may alter DNA and cell division, and nanoparticles may produce dose-dependent DNA damage, chromosomal abnormalities, and errors in chromosomal segregation, as well as the development of sister chromatic exchanges [60]. Our findings are consistent with prior research indicating that cancer cells treated with IONPs produce micronuclei [51]. As a result, we discovered that IONPs cause DNA fragmentation and, subsequently apoptosis in MCF 7 cells.

IONP treatment impairs expression of genes involved in mitochondrial function and cell apoptosis

Cells with the 50% inhibitory concentration of IONPs (5 μg/mL) to discover which genes were affected by IONP treatment, and then we did RNA-Seqeuence analysis, generating 27 million reads of RNA-Seqe data in each sample. In IONP-treated MCF 7 cells, 257 up regulated and 175 down regulated genes were denoted with cut-off values of fragments per kilobase of transcript per million mapped reads (FPKM) >2, and fold changes >2 **(Figure 7A)**. **Figure 7B** depicts examples of up-regulated (*CYP1A1 and CYP1B1*) and down-regulated (*CCNB1 and CCNB2*) genes after IONP treatment. To discover biological processes, both up and down regulated genes were subjected to Gene Ontology (GO) term analysis. The most important biological processes were drug reactions, oxidation-reduction processes, cellular responses to cadmium ions, and cell cycle regulation **(Figure 7C).** Following that, each up- or down-regulated gene was submitted to a GO term analysis. The results of the cellular and molecular analyses are supported by the findings of this study. The most highly rated biological process with up regulated genes was oxidation-reduction, as depicted in **Figures 7D and 7E**, while the most highly ranked biological process with down regulated genes was

© Under License of Creative Commons Attribution 3.0 License

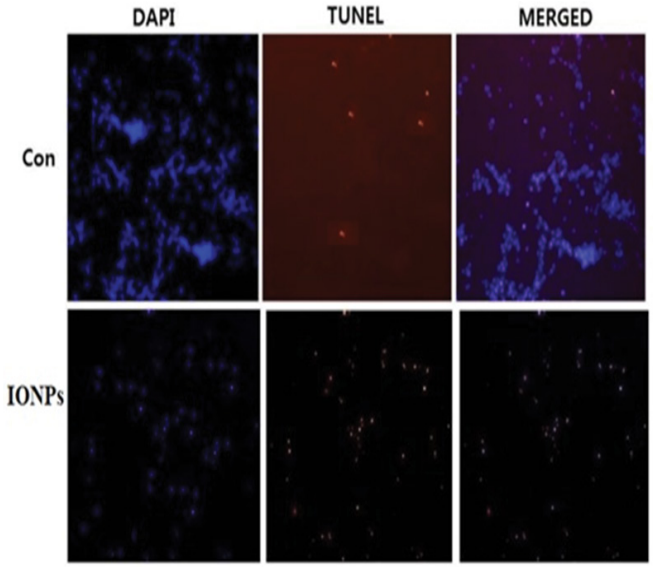

Figure 6 IONP-induced apoptosis in MCF 7 cells. The terminal deoxynucleotidyltransferase-mediated dUTP nick end labelling (TUNEL) test was then used to determine cell apoptosis, nuclei were counterstained with 40, 6-Diamidino-2-Phenylindole (DAPI) apoptotic DNA (red staining) and cell nuclei (blue staining). Original magnification is × 100, scale bar is 100 μm.

cell cycle regulation.

The oxidation-reduction related genes, in particular, code for cytochrome P450 monooxygenases such as *CYP1A1 and CYP1B1*. Cytochrome P450 enzymes are found largely in the endoplasmic reticulum and mitochondria and catalyse many of the processes involved in steroid and cholesterol production as well as drug metabolism. Previous research has linked mitochondrial *CYP1B1* to melatonin-induced apoptosis in the SH-SY5Y neuroblastoma cell line. Melatonin is known widely for its double role in apoptosis, antitumorigenic effects have been seen in some cancer cells by inducing apoptosis, although little or no effect has been seen in normal cells. Forced expression of *CYP1A1* in cancer cells resulted in cell death, which was consistent with our findings. Asik et al. [61] have found that giving a high dose of cobalt ferrite magnetic nanoparticles to human breast cancer cell lines causes cell death and increases *CYP1A1* and *CYP1B1* expression. In IONP-treated cells, genes associated with ageing were preferentially up-regulated. In comparison, G2/M check-point regulators such as *CCNB1* and *CCNB2* have been discovered in the biological process of cell cycle control with down-regulated genes.

IONP treatment dysregulates multiple biological pathways

To investigate the biological pathways linked with the differentially expressed genes, a KEGG pathway assay was performed. Down regulated genes were found to have p53 signalling and cell-cycle pathways, whereas up regulated genes had mineral absorption and metabolic pathways, as depicted in **Figures 8A and 8B.** Surprisingly, the p53 pathway has been found in both up- regulated and down-regulated genes. GTSE1, an S/G2 phase-specific gene in the p53 pathway that is an IONPs-mediated repressed gene, promotes p53 degradation by generating a protein complex. Furthermore, increased GTSE1 gene expression has been seen in numerous types of cancer, including lung cancer, myeloma cells, and gastric cancer. GADD45G, a p53 down-stream regulator, has been demonstrated to be down-regulated in a variety of cancers. Hsu et al. [62,63] stated that treatment with a natural substance,

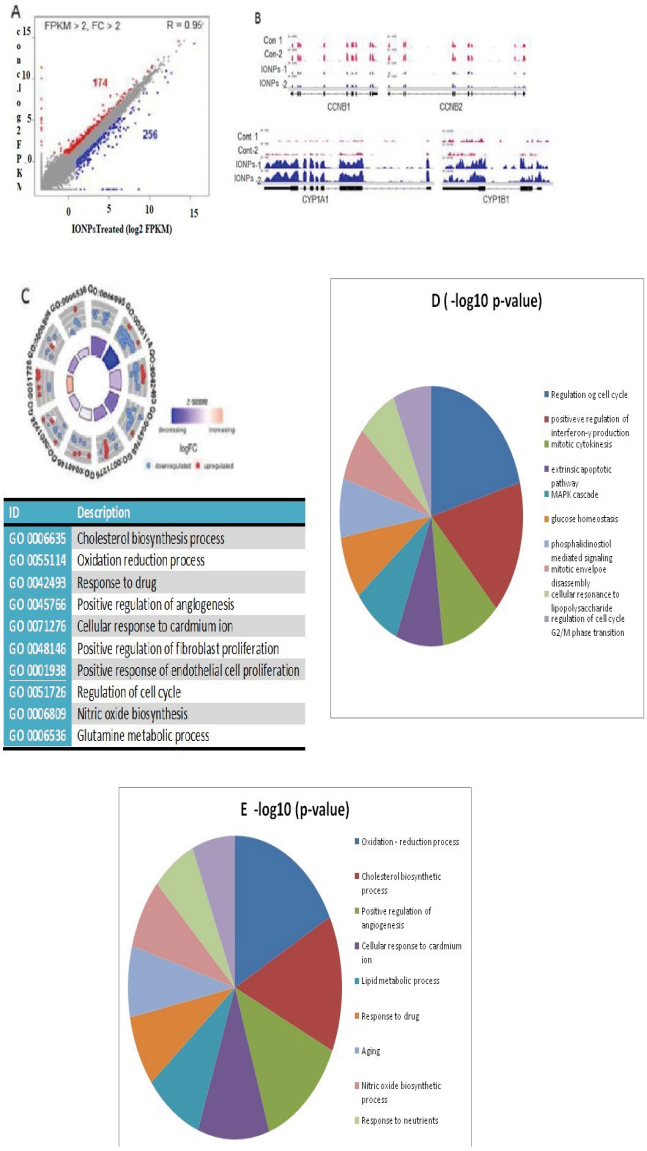

ID	Description
GO 0006635	Cholesterol biosynthesis process
GO 0055114	Oxidation reduction process
GO 0042493	Response to drug
GO 0045766	Positive regulation of anglogenesis
GO 0071276	Cellular response to cardmium ion
GO 0048146	Positive regulation of Fibroblast proliferation
GO 0001938	Positive response of endothelial cell proliferation
GO 0051726	Regulation of cell cycle
GO 0006809	Nitric oxide biosynthesis
GO 0006536	Glutamine metabolic process

Figure 7 Impact of IONPs on gene expression. (A) Scatter plot showing up-regulated and down-regulated genes in IONP-treated MCF 7 cells. Red dots indicate down-regulated and blue dots indicate up-regulated genes in IONP-treated MCF 7 cells, (B) IGV image of down-regulated gene (*CCNB1 and CCNB2*) and up-regulated gene (*CYP1A1 and CYP1B1*), (C) Gene Ontology term analysis using both up-regulated and down-regulated genes. Each dot i.e., red dot (down-regulated) and blue dot (up-regulated) represents one gene belonging to each term and (D and E) Graphs showing Gene Ontology terms of individual up-regulated and down-regulated genes.

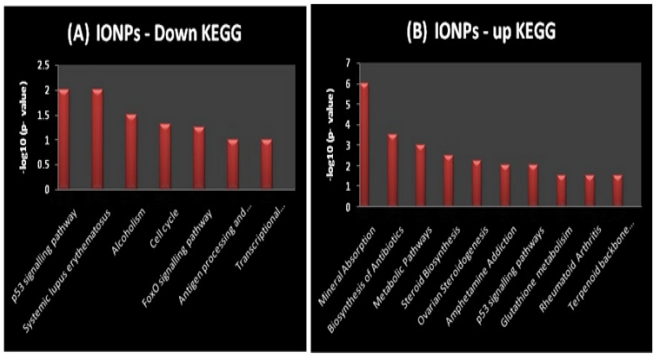

Figure 8 KEGG analysis pathway. (A) Biological pathways associated with down-regulated genes following IONP administration and (B) Biological pathways associated with Up-regulated genes following IONP administration.

cucurbitacin E, triggers G2/M arrest in GBM 8401 malignant glioma cells. GADD45G was identified in the p53 pathway, along with genes up-regulated by IONPs, according to our KEGG study. Our findings are consistent with that of Gurunathan et al. [15], who found p53 involvement and a key function for p53 up-regulation in IONP-mediated cell death in human breast cancer cells. As a result, our genome-wide investigation reveals that IONPs' tumor-suppressive action is mediated by a combination of cell apoptosis caused by DNA damage and mitochondrial dysfunction and cell cycle arrest caused by aberrant regulation of p53 effector proteins.

Conclusion

Despite increasing attention to the anti-cancer properties of IONPs, research into the possible impacts and molecular mechanisms of IONPs in cancer is limited. As a result, the main aim and objective of this investigation was to analyse the molecular mechanism of IONP exposure in human breast cancer cells using RNA-Seqe. The human MCF 7 cell line was treated for 24 hours with 2-10 μg/mL IONPs (7 nm), followed by several cellular assays and RNA-Seqeuence analysis. To evaluate the effective anticancer activity of IONPs, we synthesised them with NAR, a flavonoid found primarily in grapefruit. MCF7 cells were treated to IONPs for 24hrs and showed a dose-dependent decrease of viability and proliferation. The IC50 of 5 g/mL IONPs significantly increases LDH leakage, ROS production, and MDA levels while significantly lowering dead-cell protease activity and ATP production. By disrupting mitochondrial activity and inducing DNA damage, these events led cell death. IONPs also up-regulate and down-regulate the most highly ranked biological processes of oxidation-reduction and cell cycle regulation, respectively, according to our findings. GADD45G was found in the p53 pathway, with genes up-regulated by IONPs, according to our KEGG study.

As a result, our findings imply that IONPs' tumor-suppressive action is mediated by a combination of DNA damage-induced cell apoptosis, mitochondrial malfunction, and cell cycle arrest caused by aberrant regulation of p53 effector proteins. Following IONPs exposure, transcriptomic analysis revealed that a large number of genes, 257 up regulated and 175 down regulated, were differently expressed, significant impacts were detected in genes related to oxidation-reduction and cell cycle regulation. The p53 pathway was identified as one of the damaged pathways after down-stream analysis of the transcriptomics data. In conclusion, our analysis revealed that IONP exposure causes cell death via DNA damage, mitochondrial dysfunction, and cell-cycle arrest via aberrant regulation of p53 effector proteins, utilising a combination of RNA-Seqe and functional assays. Furthermore, gene-expression profiling technologies like RNA-Seqe can be utilised to predict IONP toxicity pathways. The molecular mechanism of IONPs' anti-cancer activity was discovered by GO studies. The study revealed that transcriptome analysis can reveal the molecular mechanism of biogenic IONPs' anti-cancer effect.

Funding

This work was supported by a grant from the DST-INSPIRE MST New-Delhi.

Acknowledgments

This study was supported by the UDPS, Utkal University.

Conflicts of Interest

The authors declare no conflict of interest.

© Under License of Creative Commons Attribution 3.0 License

References

1 Arnold M, Sierra MS, Laversanne M, Soerjomataram I, Jemal A, et al. (2017) Global patterns and trends in colorectal cancer incidence and mortality. Gut 66: 683-691.

2 Navarro M, Nicolas A, Ferrandez A, Lanas A (2017) Colorectal cancer population screening programs worldwide in 2016: An update. World J Gastroenterol 23: 3632-3642.

3 Marley AR and Nan H (2016) Epidemiology of colorectal cancer. Int J Mol Epidemiol Genet 7: 105-114.

4 Kelly C, Bhuva N, Harrison M, Buckley A, Saunders M, et al. (2013) Use of Raltitrexed as an alternative to 5-fluorouracil and Capecitabine in cancer patients with cardiac history. Eur J Cancer 49: 2303-2310.

5 Kanterman J, Sade-Feldman M, Biton M, Ish-Shalom E, Lasry A, et al. (2014) Adverse immunoregulatory effects of 5FU and CPT11 chemotherapy on myeloid-derived suppressor cells and colorectal cancer outcomes. Cancer Res 74: 6022-6035.

6 Qasim M, Lim DJ, Park H, Na D (2014) Nanotechnology for diagnosis and treatment of infectious diseases. J Nanosci Nanotechnol 14: 7374-7387.

7 De Matteis V, Cascione M, Toma CC, Leporatti S (2018) Silver nanoparticles: Synthetic routes, *in vitro* toxicity and theranostic applications for cancer disease. Nanomaterials 8: 319.

8 Zhang XF, Liu ZG, Shen W, Gurunathan S, (2016) Silver nanoparticles: Synthesis, characterization, properties, applications, and therapeutic approaches. Int J Mol Sci 17: 1534.

9 AbdelRahim K, Mahmoud SY, Ali AM, Almaary KS, Mustafa AEZMA, et al. (2017) Extracellular biosynthesis of silver nanoparticles using *Rhizopus stolonifer*. Saudi J Biol Sci 24: 208-216.

10 De Lima R, Seabra AB, Durán N (2012) Silver nanoparticles: A brief review of cytotoxicity and genotoxicity of chemically and biogenically synthesized nanoparticles. J Appl Toxicol 32: 867-879.

11 Gurunathan S, Lee KJ, Kalishwaralal K, Sheikpranbabu S, Vaidyanathan R, et al. (2009) Antiangiogenic properties of silver nanoparticles. Biomaterials 30: 6341-6350.

12 Sriram MI, Kanth SBM, Kalishwaralal K, Gurunathan S (2010) Antitumor activity of silver nanoparticles in Dalton's lymphoma ascites tumor model. Int J Nanomed 5: 753-762.

13 Guo D, Zhu L, Huang Z, Zhou H, Ge Y, et al. (2013) Anti-leukemia activity of PVP-coated silver nanoparticles via generation of reactive oxygen species and release of silver ions. Biomaterials 34: 7884-7894.

14 Gurunathan S, Han JW, Eppakayala V, Jeyaraj M, Kim JH, et al. (2013) Cytotoxicity of biologically synthesized silver nanoparticles in MDA-MB-231 human breast cancer cells. Biomed Res Int 2013: 535796.

15 Gurunathan S, Jeong JK, Han JW, Zhang XF, Park JH, et al. (2015) Multidimensional effects of biologically synthesized silver nanoparticles in Helicobacter pylori, Helicobacter felis, and human lung (L132) and lung carcinoma A549 cells. Nanoscale Res Lett 10: 35.

16 Gurunathan S, Han JW, Park JH, Kim E, Choi YJ, et al. (2015) Reduced grapheme oxide-silver nanoparticle nanocomposite: A potential anticancer nanotherapy. Int J Nanomed 10: 6257-6276.

17 Han J, Gurunathan S, Jeong JK, Choi YJ, Kwon DN, et al. (2014) Oxidative stress mediated cytotoxicity of biologically synthesized silver nanoparticles in human lung epithelial adenocarcinoma cell line. Nanoscale Res Lett 9: 459.

18 Online VA, Sahu S, Sinha N, Bhutia SK, Majhi M, et al. (2014) Luminescent magnetic hollow mesoporous silica nanotheranostics for camptothecin delivery and multimodal imaging. J Mater Chem B 3799-3808.

19 Jagannath CV and Radheshyam BK (2017) Potentiation of antiepileptic activity of phenytoin using carotene against maximal electroshock induced convulsions in mice. World J Pharm Pharm Sci 1574-1585.

20 Look M, Bandyopadhyay A, Blum JS, Fahmy TM (2010) Application of nanotechnologies for improved immune response against infectious diseases in the developing world. Adv Drug Deliv Rev 62: 378-393.

21 Feliu N, Kohonen P, Ji J, Zhang Y, Karlsson HL, et al. (2015) Next-generation sequencing reveals low-dose effects of cationic dendrimers in primary human bronchial epithelial cells. ACS Nano 9: 146-163.

22 Liu Y, Guo Y, Ma C, Zhang D, Wang C, et al. (2016) Transcriptome analysis of maize resistance to Fusarium graminearum. BMC Genom 17: 477.

23 Sun QL, Zhao CP, Wang TY, Hao XB, Wang XY, et al. (2015) Expression profile analysis of long non-coding RNA associated with vincristine resistance in colon cancer cells by next-generation sequencing. Gene 572: 79-86.

24 Morrissy AS, Garzia L, Shih DJH, Zuyderduyn S, Huang X, et al. (2016) Divergent clonal selection dominates medulloblastoma at recurrence. Nature 529: 351-357.

25 Cong L, Ran FA, Cox D, Lin S, Barretto R, et al. (2013) Multiplex genome engineering using CRISPR/Cas systems. Science 339: 819-823.

26 Kanno S, Shouji A, Hirata R, Asou K, Ishikawa M, et al. (2004) Effects of Naringin on cytosine arabinoside (Ara-C)-induced cytotoxicity and apoptosis in P388 cells. Life Sci 75: 353-365.

27 Song HM, Park GH, Eo HJ, Lee JW, Kim MK, et al. (2015) Anti-Proliferative Effect of Naringenin through p38-Dependent Downregulation of Cyclin D1 in Human Colorectal Cancer Cells. Biomol Ther(Seoul) 23: 339-344.

28 Sahu N, Soni D, Chandrashekhar B, Satpute DB, Saravanadevi S, et al. (2016) Synthesis of silver nanoparticles using flavonoids: Hesperidin, naringin and diosmin, and their antibacterial effects and cytotoxicity. Int Nano Lett 6: 173-181.

29 Shankar SS, Rai A, Ahmad A, Sastry M (2004) Rapid synthesis of Au, Ag, and bimetallic Au core-Ag shell nanoparticles using Neem (Azadirachta indica) leaf broth. J Colloid Interface Sci 275: 496-502.

30 Jain S and Mehata MS (2017) Medicinal plant leaf extract and pure flavonoid mediated green synthesis of silver nanoparticles and their enhanced antibacterial property. Sci Rep 7: 15867.

31 Singhal G, Bhavesh R, Kasariya K, Sharma AR, Singh RP, et al. (2011) Biosynthesis of silver nanoparticles using Ocimum sanctum (Tulsi) leaf extract and screening its antimicrobial activity. J Nanopart Res 13: 2981-2988.

32 Verma A and Mehata MS (2016) Controllable synthesis of silver nanoparticles using Neem leaves and their antimicrobial activity. J Radiat Res Appl Sci 9: 109-115.

33 Prathna TC, Chandrasekaran N, Raichur AM, Mukherjee A, (2011) Biomimetic synthesis of silver nanoparticles by *Citrus limon* (lemon) aqueous extract and theoretical prediction of particle size. Colloids Surf B Biointerfaces 82: 152-159.

34 Rumpker R, Richter M, Kjeldsen F, Brewer J, Hoyland J, et al. (2014)

Exposure to silver nanoparticles induces size- and dose-dependent oxidative stress and cytotoxicity in human colon carcinoma cells. Toxicol *In Vitro* 28: 1280-1289.

35 Durai P, Chinnasamy A, Gajendran B, Ramar M, Pappu S, et al. (2014) Synthesis and characterization of silver nanoparticles using crystal compound of sodium para-hydroxybenzoate tetrahydrate isolated from *Vitex negundo L*. leaves and its apoptotic effect on human colon cancer cell lines. Eur J Med Chem 84: 90-99.

36 Satapathy SR, Mohapatra P, Preet R, Das D, Sarkar B, et al. (2013) Silver-based nanoparticles induce apoptosis in human colon cancer cells mediated through p53. Nanomedicine 8: 1307-1322.

37 Mata R, Nakkala JR, Sadras SR (2015) Biogenic silver nanoparticles from *Abutilon indicum*: Their antioxidant, antibacterial and cytotoxic effects *in vitro*. Colloids Surf. B Biointerfaces 128: 276-286.

38 Azizi M, Ghourchian H, Yazdian F, Bagherifam S, Bekhradnia S, et al. (2017) Anti-cancerous effect of albumin coated silver nanoparticles on MDA-MB 231 human breast cancer cell line. Sci Rep 7: 5178.

39 Yuan YG, Wang YH, Xing HH, Gurunathan S (2017) Quercetin-mediated synthesis of graphene oxide-silver nanoparticle nanocomposites: A suitable alternative nanotherapy for neuroblastoma. Int J Nanomed 12: 5819-5839.

40 Burd JF and Usategui-Gomez M (1973) A colorimetric assay for serum lactate dehydrogenase. Clin Chim Acta 46: 223-227.

41 Chan FKM, Moriwaki K, De Rosa MJ (2013) Detection of necrosis by release of lactate dehydrogenase activity. Methods Mol Biol 979: 65-70.

42 Castiglioni S, Caspani C, Cazzaniga A, Maier JA (2014) Short- and long-term effects of silver nanoparticles on human microvascular endothelial cells. World J Biol Chem 5: 457-464.

43 Brayner R (2008) The toxicological impact of nanoparticles. Nano Today 3: 48-55.

44 Yuan YG, Peng QL, Gurunathan S (2017) Silver nanoparticles enhance the apoptotic potential of gemcitabine in human ovarian cancer cells: Combination therapy for effective cancer treatment. Int J Nanomed 12: 6487-6502.

45 Han JW, Gurunathan S, Choi YJ, Kim JH (2017) Dual functions of silver nanoparticles in F9 teratocarcinoma stem cells, a suitable model for evaluating cytotoxicity- and differentiation-mediated cancer therapy. Int J Nanomed 12: 7529-7549.

46 Han JW, Jeong JK, Gurunathan S, Choi YJ, Das J, et al. (2016) Male- and female-derived somatic and germ cell-specific toxicity of silver nanoparticles in mouse. Nanotoxicology 10: 361-373.

47 Buttacavoli M, Albanese NN, di Cara G, Alduina R, Faleri C, et al. (2018) Anticancer activity of biogenerated silver nanoparticles: An integrated proteomic investigation. Oncotarget 9: 9685-9705.

48 Travan A, Pelillo C, Donati I, Marsich E, Benincasa M, et al. (2009) Non-cytotoxic silver nanoparticle-polysaccharide nanocomposites with antimicrobial activity. Biomacromolecules 10: 1429-1435.

49 Pelicano H, Carney D, Huang P (2004) ROS stress in cancer cells and therapeutic implications. Drug Resist Updat 7: 97-110.

50 Gliga AR, di Bucchianico S, Lindvall J, Fadeel B, Karlsson HL, et al. (2018) RNA-sequencing reveals long-term effects of silver nanoparticles on human lung cells. Sci Rep 8: 6668.

51 AshaRani PV, Low Kah Mun G, Hande MP, Valiyaveettil S (2009) Cytotoxicity and genotoxicity of silver nanoparticles in human cells. ACS Nano 3: 279-290.

52 Choi YJ, Park JH, Han JW, Kim E, Lee SY, et al. (2016) Differential cytotoxic potential of silver nanoparticles in human ovarian cancer cells and ovarian cancer stem cells. Int J Mol Sci 17: 2077.

53 Zhang XF, Shen W, Gurunathan S (2016) Silver nanoparticle-mediated cellular responses in various cell lines: An *in Vitro* model. Int J Mol Sci 17: 1603.

54 Orlowski P, Krzyzowska M, Zdanowski R, Winnicka A, Nowakowska J, et al. (2013) Assessment of *in vitro* cellular responses of monocytes and keratinocytes to tannic acid modified silver nanoparticles. Toxicol *In Vitro* 27: 1798-1808.

55 Maurer LL and Meyer JN (2016) A systematic review of evidence for silver nanoparticle-induced mitochondrial toxicity. Environ Sci Nano 3: 311-322.

56 Neustadt J and Pieczenik SR (2008) Medication-induced mitochondrial damage and disease. Mol Nutr Food Res 52: 780-788.

57 Navarro E, Piccapietra F, Wagner B, Marconi F, Kaegi R (2008) Toxicity of silver nanoparticles to Chlamydomonas reinhardtii. Environ Sci Technol 42: 8959-8964.

58 Schieber M and Chandel NS (2014) ROS function in redox signaling and oxidative stress. Curr Biol 24: R453-R462.

59 Elmore S (2007) Apoptosis: A Review of Programmed Cell Death. Toxicol Pathol 35: 495-516.

60 Liu F, Mahmood M, Xu Y, Watanabe F, Biris AS, et al. (2015) Effects of silver nanoparticles on human and rat embryonic neural stem cells. Front Neurosci 9: 115.

61 A¸sık E, Aslan TN, Volkan M, Güray NT (2016) 2-Amino-2-deoxy-glucose conjugated cobalt ferrite magnetic nanoparticle (2DG-MNP) as a targeting agent for breast cancer cells. Environ. Toxicol Pharmacol 41: 272-278.

62 Hsu YC, Chen MJ, Huang TY (2014) Inducement of mitosis delay by *Cucurbitacin E*, a novel tetracyclic triterpene from climbing stem of *Cucumis melo L*, through GADD45 in human brain malignant glioma (GBM) 8401 cells. Cell Death Dis 5: e1087.

63 Hsu YC, Huang TY, Chen MJ (2014) Therapeutic ROS targeting of GADD45 in the induction of G2/M arrest in primary human colorectal cancer cell lines by *Cucurbitacin E*. Cell Death Dis 5: e1198.

© Under License of Creative Commons Attribution 3.0 License